Terr. Atmos. Ocean. Sci., Vol. 27, No. 6, 825-836, December 2016 doi: 10.3319/TAO.2016.02.04.01(TT)

East Asian Monsoon Precipitation and Paleoclimate Record Since the Last Interglacial Period in the Bohai Sea Coastal Zone, China

Shuhuan Du[1], Baosheng Li[2, 3, *], Zhiwen Li[4], Muhong Chen[1], David Dian Zhang[5], Rong Xiang[1], Dongfeng Niu[2], and Yuejun Si[6]

[1] *Key Laboratory of Marginal Sea Geology, South China Sea Institute of Oceanology, Chinese Academy of Sciences, Guangzhou, China*
[2] *Department of Geography, South China Normal University, Guangzhou, China*
[3] *State Key Laboratory of Loess and Quaternary Geology, Institute of Earth Environment, Chinese Academy of Sciences, Xi'an, China*
[4] *College of Earth Sciences, East China Institute of Technology, Nanchang, China*
[5] *Department of Geography, University of Hong Kong, Pokfulam Road, Hong Kong, China*
[6] *School of Geography and Planning, Guangxi Teachers Education University, Nanning, China*

Received 10 October 2015, revised 3 February 2016, accepted 4 February 2016

ABSTRACT

The Miaodao stratigraphic section (MDS) is located in the Bohai Sea, coastal zone of China, and holds historical information about regional climatic features, sea-level changes, and evolution of the East Asian monsoon. By analyzing the ages of the various sedimentary fascia, combined with proxy paleoclimatic indices [i.e., average grain size (Mz), clay + silt/sand content (SC/D), grain < 0.63 μm fraction, CIA value, and Si_2O/Al_2O_3 and Rb/Sr ratios], we conclude that the aeolian deposit in the MDS has been directly driven by the East Asian monsoon since the last interglacial period. The grain < 0.63 μm fraction of the MDS, as demonstrated by monsoon precipitation indices, indicates multiple rainfall fluctuations in the Bohai Sea coastal zone since the last interglacial period, marine isotope stage 5e (MIS5e), when the strongest centennial-scale rainfall occurred. Evidence can be found in the stalagmite record from Shanbao Cave in the Shennongjia nature reserve. The Holocene Climatic Optimum was a period of persistent monsoon precipitation when the precipitation intensity ranked second only to MIS5e. These analyses results indicate that the MDS sediment and monsoon precipitation are controlled by the East Asian monsoon, resulting in sea-level fluctuations.

Key words: East Asian monsoon, Monsoon precipitation, Paleoclimate, Miaodao Section, Last interglacial

Citation: Du, S., B. Li, Z. Li, M. Chen, D. D. Zhang, R. Xiang, D. Niu, and Y. Si, 2016: East Asian monsoon precipitation and paleoclimate record since the last interglacial period in the Bohai Sea coastal zone, China. Terr. Atmos. Ocean. Sci., 27, 825-836, doi: 10.3319/TAO.2016.02.04.01(TT)

1. INTRODUCTION

Several studies have documented changes in the East Asian Monsoon since the last interglacial period, coincident with marine isotope stage 5e (MIS5e). These changes have been documented in terrestrial records such as loess-paleosol deposits in northern China (Liu 1985; Porter and An 1995; An 2000), aeolian deposits in north-central China (Li et al. 2000; Du et al. 2011, 2012), lacustrine deposits in northern and southern China (Shen et al. 2005; Zhong et al. 2010), and stalagmites in southern and eastern China (Wang et al. 2001; Yuan et al. 2004). However, research conducted on records from the coastal environment has been insufficient. This paper presents a record of East Asian Monsoon behavior since approximately 130 ka from the Bohai Sea coastal zone in eastern China. Most previous studies from the Bohai Sea coastal zone have concentrated on the last glacial period and the Holocene Epoch and lack robust chronological frameworks. Wang et al. (2007), for example, investigated magnetic and carbonate loess content in the coastal zone and found evidence of four previous climate fluctuations in this area. Li et al. (2008) measured the magnetic susceptibility of the loess and compared these data with the climate records from ice cores from Greenland. Xu (2008, 2010) studied the grain-size characteristics of the loess and inferred that

* *Corresponding author*
E-mail: libsh@scnu.edu.cn

six climate fluctuations occurred during the last glacial period. This paper presents the Miaodao stratigraphic section (MDS), which is composed of sediments that accumulated since approximately 130 ka. The description and interpretation of this section yields insight into the characteristics and impact of the East Asian monsoon on the Bohai Sea coastal zone and provides a foundation for a comprehensive and overall understanding of the evolution of ancient monsoons in the eastern monsoon region of China.

2. REGIONAL SETTING

The MDS is located at 37°56'31.9"N, 120°40'35.9"E at an elevation of 17 m above sea level in the northwest region of the Miaodao Archipelago in the Bohai Sea (Fig. 1). At this site, approximately 6.5 m of Quaternary sediments rest on an unconformity above weathered granitoid crust (Fig. 2). The average annual temperature in the Miaodao Archipelago is 11 - 12°C, and the average annual rainfall is 700 - 800 mm (Shandong Changdao County Compilation Committee 1990). The rainfall increases up to 81% of the annual precipitation during the summer and autumn seasons and up to 19% during the winter and spring (Shandong Changdao County Compilation Committee 1990).

3. METHODS AND MATERIALS

3.1 AMS-^{14}C and OSL Age Test

We obtained 12 sets of age data, including 3 sets of accelerator mass spectrometry radiocarbon dating (AMS-^{14}C) data and 9 optically stimulated luminescence (OSL) datasets from 10 layers in the MDS (Fig. 2). The AMS-^{14}C age determination was completed in the AMS-^{14}C Key Laboratory of Nuclear Physics and Technology at Beijing University. The OSL procedure was conducted using the following two instruments and locations: the Daybreak 2200 OSL reader in the OSL Laboratory of the Institute of Hydrogeology and Environmental Geology, Chinese Academy of Geological Sciences and the 1100B OSL instrument in the Isotope and OSL Dating Laboratory of the Department of Earth Sciences, Sun Yat-sen University (Daybreak Nuclear and Medical Systems, Inc., USA). The OSL sample tubes were opened under a subdued red light in the laboratory. The surface sample at both ends of the tube was scraped away

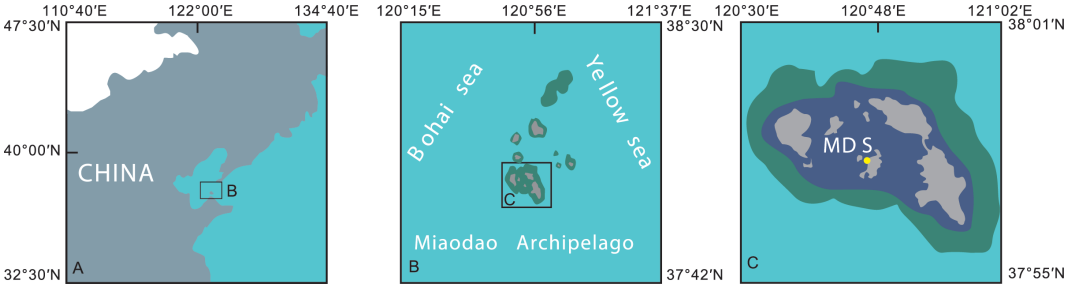

Fig. 1. Location of the MDS. (Color online only)

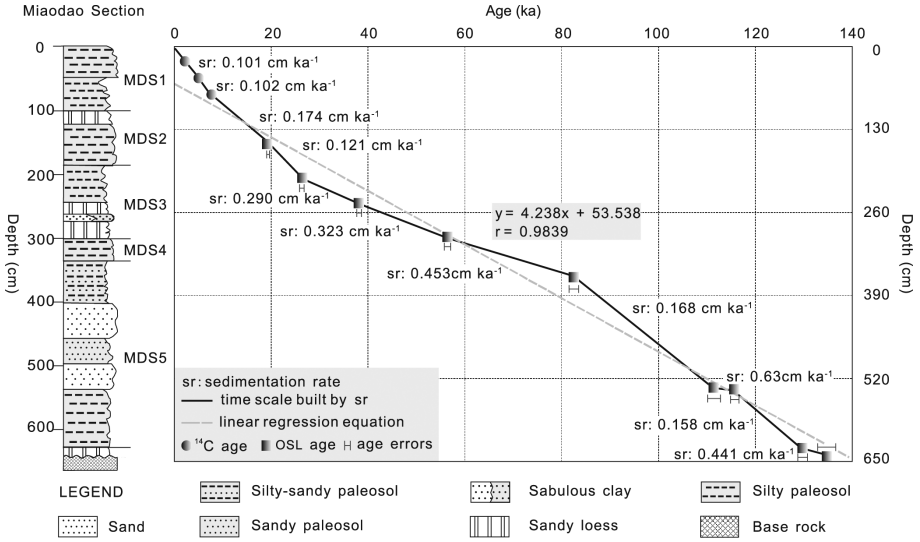

Fig. 2. Sequence and timescale of the MDS since MIS5e.

for moisture content, radionuclide concentration, and other proxy measurements. Only the central part of the sediment was used for OSL dating to avoid any incidental exposure to light during sampling and transportation. The samples were treated with 10% HCl and 30% H_2O_2 to remove carbonates and organics, respectively. Quartz minerals were extracted using heavy liquid separation with sodium polytungstate and were subsequently treated with 40% hydrofluoric acid (HF) for approximately 60 min to etch the grain surfaces and dissolve any remaining feldspar minerals. The grain-size fraction of 4 - 11 μm was extracted by wet sieving. The resulting quartz grains were washed with 10% HCl to remove fluoride precipitates. Quartz grain purity was checked using infrared stimulation at 830 nm. Any samples with obvious infrared stimulated luminescence (IRSL) signals were retreated with H_2SiF_6 to avoid equivalent dose (De) underestimation (Lai et al. 2008). The pretreated grains were then mounted on 0.1-cm-diameter center parts of stainless steel disks 9.7 mm in diameter using silicone oil. This process involved preheating the samples to 260°C for 10 s before measuring the natural and regenerative doses of radiation and preheating to 220°C for 10 s before measuring each test dose of radiation. Each grain was optically stimulated for 2 s at 125 °C using a focused green laser beam. At the end of each measurement cycle the grains were optically stimulated for 60s using blue light-emitting diodes while being held at 280°C (Jacobs et al. 2006; Wintle and Murray 2006). Organic matter was used as the test material for the AMS-^{14}C test, in which the ^{14}C age results that were corrected through the CALIB 5.01 program and the IntCal04 database (Stuiver et al. 1998) showed a range of 0 - 21.381 ka with a 138 error of 2σ.

3.2 Grain Size

A total of 314 samples of various grain sizes were obtained from the MDS at 2-cm intervals from top to bottom. The Malvern Mastersizer 2000 M laser grain size analyzer, with a measuring range of 0.02 - 2000 μm, was used for the grain size analysis. A chemical pretreatment was carefully conducted following the guidelines set by Konert and Vandenberghe (1997). All grain size data were stored in a database and the results were calculated using the MatLab 7.0 software. The mean grain size (Mz; Φ) of the MDS was calculated based on the formula developed by Folk and Ward (1957): Mz = (16Φ + 50Φ + 84Φ)/3. The sensitive components of the MDS were extracted through grain size using standard deviation and each layer of the SC/D [(clay + silt)/sand] value was calculated.

3.3 Chemical Elements

We collected 81 samples at 8-cm intervals to conduct geochemical analyses using an X-ray fluorescence spectrometer (Type 3070; Rigaku International Corp., Tokyo, Japan) in the Cold and Arid Regions Environment and Engineering Research Institute of the Chinese Academy of Sciences. The samples were initially dried, heated to 80°C for 24 h, then ground, sieved through a 200-mesh screen and further ground into small pieces of 30 μm in diameter for analysis. The national standard sediments, GSD9 and GSS1, were used as controls for the test results. The relative deviation and errors were both less than 5%. In this study we used the Rb/Sr ratio, SiO_2/Al_2O_3 ratio, and chemical index of alteration (CIA) value $[Al_2O_3/(Al_2O_3 + CaO + Na_2O + K_2O)] \times 100$ as the proxy paleoclimatic indices to discuss the climate environment evolution.

3.4 Scanning Electron Microscope

We used a scanning electron microscope (SEM) at the Sun Yat-sen University test center to test quartz samples from the MDS. The samples were magnified 20 to 200 times under the SEM (S-520, Japan). The quartz samples were cleaned, the organic matter and calcium carbonate were removed and the samples were examined using SEM.

4. DESCRIPTION OF THE MDS SECTION

The Quaternary section consists of 15 units, which are described below from base to top according to the lithology and depositional environment:

Unit 1, 16 cm thick, is composed of silty/very fine to fine sand with clay; mean values are 49.67% sand, 38.09% silt, and 12.24% clay. The overall Mz is 4.74 Φ, and the mean ratio of (silt + clay)/sand is 1.02 (Fig. 3). This unit is unstratified and fossils are not present. Chemical analyses of the sediments revealed that the mean ratios of SiO_2/Al_2O_3 and Rb/Sr are 8.91 and 0.59, respectively; the CIA is 68.45. This unit rests on an unconformity above weathered granitoid crust. Its upper contact is a transitional contact immediately below a bed of silty paleosol, which is described below as Unit 2.

Unit 2, 90 cm thick, is composed of fine to very fine sand/silty sand with clay; mean values are 26.63% sand, 55.23% silt, and 18.15% clay. The overall Mz is 5.63 Φ, and the mean ratio of (silt + clay)/sand is 2.96 (Figs. 3 and 4). Sedimentary structures are not apparent and fossils are not present. Chemical analyses of the sediments revealed that the mean ratios of SiO_2/Al_2O_3 and Rb/Sr are 4.75 and 0.68, respectively; CIA is 72.47. The upper contact of this unit is a transitional contact immediately below a bed of aeolian sand, which is described below as Unit 3.

Unit 3, 40 cm thick, is composed of silty fine sand; mean values are 71.61% sand, 21.11% silt, and 7.28% clay. The overall Mz is 3.65 Φ, and the mean ratio of (silt + clay)/sand is 0.40 (Fig. 3). Sedimentary structures are slightly cemented and unstratified; many pseudomycelia are present.

Chemical analyses of the sediments revealed that the mean ratios of SiO_2/Al_2O_3 and Rb/Sr are 8.09 and 0.50, respectively; CIA is 62.27. The upper contact of this unit is a transitional contact immediately below a bed of sandy paleosol, which is described below as Unit 4.

Unit 4, 40 cm thick, is composed of silty fine sand with clay; mean values are 63.39% sand, 28.90% silt, and 7.71% clay. The overall Mz is 3.88 Φ, and the mean ratio of (silt + clay)/sand is 0.59 (Fig. 3). Sedimentary structures have slight to medium cementation and are unstratified; many pseudomycelia are present. Chemical analyses of the sediments revealed that the mean ratios of SiO_2/Al_2O_3 and Rb/Sr are 7.32 and 0.51, respectively; CIA is 64.34. The upper contact of this unit is a transitional contact immediately below a bed of aeolian sand, which is described below as Unit 5.

Unit 5, 56 cm thick, is composed of silty fine sand; mean values are 66.66% sand, 27.08% silt, and 6.26% clay. The overall Mz is 3.68 Φ, and the mean ratio of (silt + clay)/sand is 0.50 (Figs. 3 and 4). Sedimentary structures are slightly cemented and unstratified; some pseudomycelia are present. Chemical analyses of the sediments revealed that the mean ratios of SiO_2/Al_2O_3 and Rb/Sr are 7.27 and 0.52, respectively; CIA is 64.15. The upper contact of this unit is a transitional contact immediately below a bed of silty to sandy paleosol, which is described below as Unit 6.

Unit 6, 66 cm thick, is composed of very fine sand/silty sand with clay and fine sand; mean values are 48.56% sand, 40.78% silt, and 10.66% clay. The overall Mz is 4.57 Φ, and the mean ratio of (silt + clay)/sand is 1.10 (Fig. 3). Sedimentary structures have slight to medium cementation and are unstratified; some pseudomycelia are present. Chemical analyses of the sediments revealed that the mean ratios of SiO_2/Al_2O_3 and Rb/Sr are 6.25 and 0.47, respectively; CIA is 58.39. The upper contact of this unit is a transitional contact immediately below a bed of silty paleosol, which is described below as Unit 7.

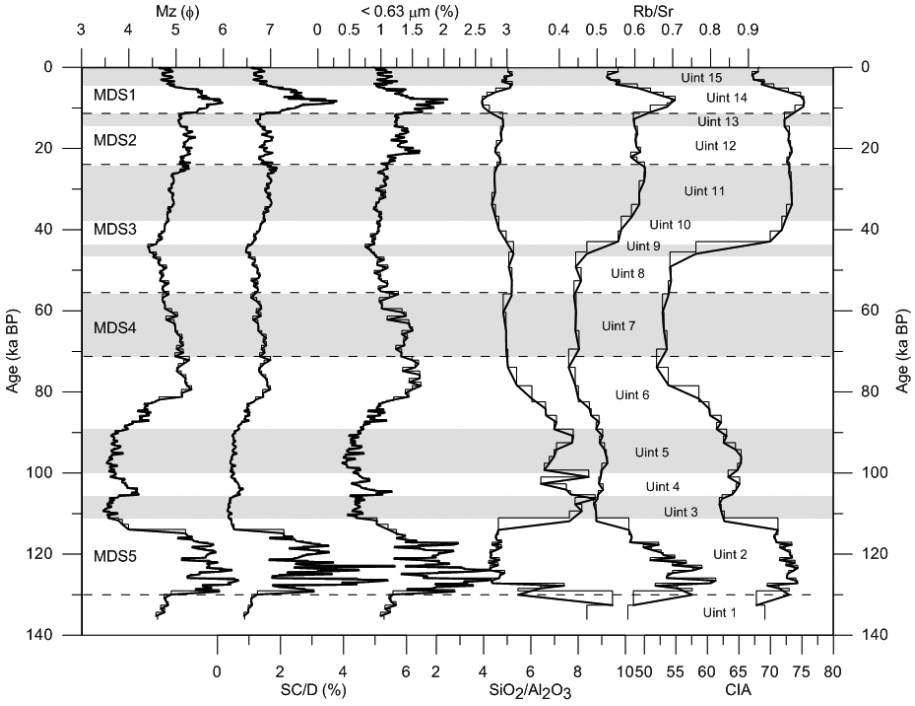

Fig. 3. Change curves of Mz (Φ), SC/D, grain < 0.63 μm fraction (%), SiO_2/Al_2O_3 ratio, CIA, and Rb/Sr ratio in the MDS.

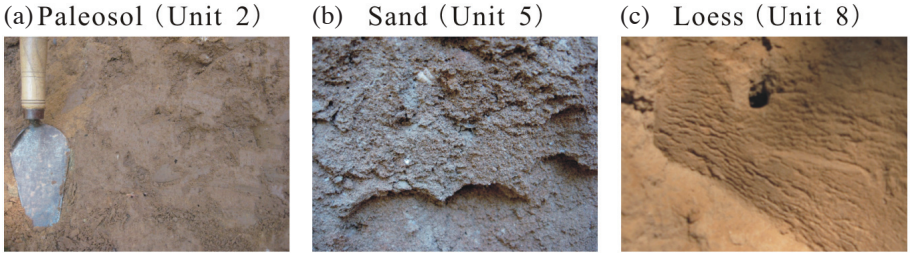

Fig. 4. Various sedimentary fascias in the Miaodao section. (a) Unit 2-paleosol face. (b) Unit 2-aeolian sand. (c) Unit 8-loess. (Color online only)

Unit 7, 34 cm thick, is composed of very fine sand/silty sand with clay and fine sand; mean values are 42.81% sand, 45.55% silt, and 11.63% clay. The overall Mz is 4.72 Φ, and the mean ratio of (silt + clay)/sand is 1.12 (Fig. 3). Sedimentary structures contain some kankar. Chemical analyses of the sediments revealed that the mean ratios of SiO_2/Al_2O_3 and Rb/Sr are 4.91 and 0.45, respectively; CIA is 53.18. The upper contact of this unit is a transitional contact immediately below a bed of sand-loess, which is described below as Unit 8.

Unit 8, 28 cm thick, is composed of very fine sand/silty sand with clay and fine sand; mean values are 44.98% sand, 46.67% silt, and 8.35% clay. The overall Mz is 4.72 Φ, and the mean ratio of (silt + clay)/sand is 1.23 (Figs. 3 and 4). Sedimentary structures are unstratified and include loose holes, kankar and pseudomycelia. Chemical analyses of the sediments revealed that the mean ratios of SiO_2/Al_2O_3 and Rb/Sr are 5.15 and 0.45, respectively; CIA is 54.03. The upper contact of this unit is a transitional contact immediately below a bed of sandy loam, which is described below as Unit 9.

Unit 9, 10 cm thick, is composed of silty/very fine sand with clay; mean values are 51.08% sand, 42.40% silt, and 6.52% clay. The overall Mz is 4.47 Φ, and the mean ratio of (silt + clay)/sand is 0.96 (Fig. 3). Sedimentary structures are unstratified and include a large amount of loose holes. Chemical analyses of the sediments revealed that the mean ratios of SiO_2/Al_2O_3 and Rb/Sr are 5.26 and 0.47, respectively; CIA is 58.19. The upper contact of this unit is a transitional contact immediately below a bed of sand-loess, which is described below as Unit 10.

Unit 10, 18 cm thick, is composed of very fine sand/silty sand with fine sand and clay; mean values are 44.44% sand, 47.76% silt, and 7.8% clay. The overall Mz is 4.69 Φ, and the mean ratio of (silt + clay)/sand is 1.25 (Fig. 3). Sedimentary structures are unstratified and include loose holes. Chemical analyses of the sediments revealed that the mean ratios of SiO_2/Al_2O_3 and Rb/Sr are 4.80 and 0.60, respectively; CIA is 70.89. The upper contact of this unit is a transitional contact immediately below a bed of silty paleosol, which is described below as Unit 11.

Unit 11, 58 cm thick, is composed of very fine sand/silty sand with clay and fine sand; mean values are 37.97% sand, 52.14% silt, and 9.89% clay. The overall Mz is 4.97 Φ, and the mean ratio of (silt + clay)/sand is 1.64 (Fig. 3). Sedimentary structures are not apparent and fossils are not present. Chemical analyses of the sediments revealed that the mean ratios of SiO_2/Al_2O_3 and Rb/Sr are 4.47 and 0.62, respectively; CIA is 73.09. The upper contact of this unit is a transitional contact immediately below a bed of silty paleosol, which is described below as Unit 12.

Unit 12, 66 cm thick, is composed of very fine sand/silty sand with fine sand and clay; mean values are 39.85% sand, 45.54% silt, and 14.61% clay. The overall Mz is 5.21 Φ, and the mean ratio of (silt + clay)/sand is 1.52 (Fig. 3). Sedimentary structures are not apparent and fossils are not present. Chemical analyses of the sediments revealed that the mean ratios of SiO_2/Al_2O_3 and Rb/Sr are 4.65 and 0.60, respectively; CIA is 73.01. The upper contact of this unit is a transitional contact immediately below a bed of sand-loess, which is described below as Unit 13.

Unit 13, 20 cm thick, is composed of very fine sand/silty sand with fine sand and clay; mean values are 42.71% sand, 43.76% silt, and 13.53% clay. The overall Mz is 5.09 Φ, and the mean ratio of (silt + clay)/sand is 1.34 (Fig. 3). This unit is unstratified and fossils are not present. Chemical analyses of the sediments revealed that the mean ratios of SiO_2/Al_2O_3 and Rb/Sr are 4.82 and 0.60, respectively; CIA is 72.23. The upper contact of this unit is a transitional contact immediately below a bed of silty paleosol, which is described below as Unit 14.

Unit 14, 52 cm thick, is composed of very fine sand/silty sand with clay; mean values are 28.10% sand, 54.72% silt, and 17.18% clay. The overall Mz is 5.60 Φ, and the mean ratio of (silt + clay)/sand is 2.63 (Fig. 3). Sedimentary structures are not apparent and fossils are not present. Chemical analyses of the sediments revealed that the mean ratios of SiO_2/Al_2O_3 and Rb/Sr are 4.26 and 0.66, respectively; CIA is 73.98. The upper contact of this unit is a transitional contact immediately below a bed of silty paleosol, which is described below as Unit 15.

Unit 15, 50 cm thick, is composed of very fine sand/silty sand with clay and fine sand; mean values are 42.55% sand, 48.12% silt, and 9.33% clay. The overall Mz is 4.83 Φ, and the mean ratio of (silt + clay)/sand is 1.36 (Fig. 3). Sedimentary structures contain many wormholes and root systems. Chemical analyses of the sediments revealed that the mean ratios of SiO_2/Al_2O_3 and Rb/Sr are 5.01 and 0.55, respectively; CIA is 67.96.

5. RESULTS

5.1 Chronology

The AMS-^{14}C specific sampling layer, depth, tree-ring calibration age and relevant parameters of the OSL are listed in Table 1. A linear regression correlation coefficient (r) of 0.98 demonstrates the relationship between age and depth in the test results in Table 1, indicating that age varies with depth. We used the known ages and segmentation sedimentation rates to establish the MDS chronology since MIS5e (Fig. 2). To compare the climatic changes in the MDS with the division scheme in the marine cores of the MIS5 to MIS1 sections and the MIS5 and MIS3 subsections, we first divided the MDS into five stratigraphic segments, MDS1, MDS2, MDS3, MDS4, and MDS5, based on the determined ages. The other ages were calculated using regression lines for the sedimentation rates (Fig. 2). Thereafter, we dated each segment based on the different sedimentation rates. As

shown in the results, the time boundary of each section and subsection in the MDS has a definite time difference from that of the marine oxygen isotope stages. However, the dating error in the OSL is between 0.26 and 6.3 ka, which is comparable to each subsection in the marine isotope stage framework.

5.2 Grain Size

The Mz analysis results in the MDS show that Mz ranges from 3.46Φ to 6.32Φ, with an average of 4.80Φ. The content is mainly sand, which varies from 11.20 - 99.08%, followed by silt at 17.96 - 75.66%, and clay at 5.22 - 25.81%. The average sand, silt and clay contents are 44.71, 43.61, and 11.68%, respectively. The SC/D value of the section ranges from 0.32 - 5.63, with a mean value of 1.51, showing large fluctuations in the sand content. The SC/D trend is similar to the Mz trend in the perpendicular direction of the section.

The Mz results reflect the average condition of the sediment grain diameter and indicate the transport intensity. Of the different sedimentary fascia, paleosol has the finest average particle size, followed by sand-loess and sandy loam. Aeolian sand is the coarsest. Although the material sources in the region during the different periods were nonconforming, the sedimentary fascia formation is reflected by the sources and related to biochemical weathering, which is closely linked to climate changes. Thus, the changes in the sedimentary fascia and Mz represent different climatic environments. This result corresponds with the Loess Plateau study results, which show that Mz is a good proxy index for representing climate change during the East Asian winter and summer monsoons (An et al. 1991; Ding et al. 1992). This proxy can also reflect the depositional environment to some extent. The SC/D trend is similar to the Mz trend in the perpendicular direction of the section. The changes in the different sedimentary fascia are the same as those for the grain size. Paleosol has the highest value, followed by sand-loess, sandy loam, and aeolian sand. The nature of the SC/D value increases the proportional relationship among the grains, > 4.32Φ/< 4.32Φ, which illustrates the two different wind directions that alternate and change strengths in the East Asian monsoon system (Wen et al. 2005). Low values indicate sand sedimentation under strong winds in a dry and cold climate, while high values indicate weakened sand activities in a warm and humid climate as well as enhanced soil weathering. Analysis of the standard deviation for each size fraction indicated two main grain size fractions in this area, represented by two obvious standard deviation peaks (Fig. 5a). These peaks correspond to the grain size fractions that range from 154 μm to 178.35 μm (component 1) and 50 - 56.368 μm (component 2). The former accounts for 0.09 - 15.5% of the whole rock and the latter can reach 2.5 - 11.5% (Fig. 5b), indicating that the section sediment sources are non-uniform.

5.3 Chemical Elements

The MDS chemistry was analyzed using the SiO_2/Al_2O_3 ratio, CIA value and Rb/Sr ratio as proxy paleoclimatic indices. The ranges and average of these three indices in the section are as follows: SiO_2/Al_2O_3 ratio, 3.93 to 8.72, 5.34; CIA value, 51.94 to 75.34, 67.94; and Rb/Sr ratio, 0.42 to 0.81, 0.59. The SiO_2/Al_2O_3 ratio trend is almost opposite the CIA value and Rb/Sr ratio trends: When the SiO_2/Al_2O_3 ratio curve peaks, the CIA value and Rb/Sr ratio curves reach their minima and vice versa. However, the CIA value and Rb/Sr ratio trends are more consistent with the relatively large amplitude of the CIA change. The change curves of Mz (Φ), SC/D, and other indices are presented in Fig. 3.

The SiO_2/Al_2O_3 ratio reflects the degree of weathering in the sediments represented by the quartz abundance and clay-to-feldspar ratio (Potter 1978). Aeolian sand (paleosol) has the highest (lowest) SiO_2/Al_2O_3 ratio in different sedimentary fascia. Generally, when the climate is humid and hot, the relative Fe and Al enrichment results from SiO_2 leaching, thereby reducing the SiO_2/Al_2O_3 ratio. Conversely, less SiO_2 leaching occurs in an arid climate, resulting in a higher SiO_2/Al_2O_3 ratio. The CIA indicates the degree to which surface rocks undergo chemical weathering. This index mainly reflects the silicate minerals in which feldspar is dominant. High CIA values indicate significant chemical weathering intensity. The Rb/Sr ratio has been positively correlated with the weathering intensity (Dasch 1969). Moreover, Chen et al. (1999) adopted the Rb/Sr ratio to indicate climatic variations during the formation periods of loess and paleosol in the Loess Plateau. This ratio can accurately indicate the intensity of winter and summer monsoons (Pang et al. 2001). In the MDS, paleosol has the highest CIA value and Rb/Sr ratio, indicating a formation interval with a strong degree of chemical weathering. Conversely, the development periods of the sandy loam and aeolian sand are associated with weak chemical weathering in addition to a lower CIA value and Rb/Sr ratio.

6. DISCUSSION

6.1 Sediment Source of the MDS

The standard MDS deviation was analyzed with two sensitive components found. To clarify the MDS sediment source, Fig. 5c shows grain-size cumulative probability curves drawn for each section from MDS1 to MDS5. These curves are multistage, including three-component tractions, saltation, and suspension, and they illustrate the diversity of the sediment sources in the sections. The suspended component is composed of a clay fraction > 10.5Φ (< 0.63 μm) and a silt group > 4Φ, in which the clay fraction content is relatively stable and ranges from 0.54 - 3.63% with an average content of 1.55%. We then attempted to identify the clay fraction source with grain size < 0.63 μm in the

MDS. Shepard et al. (1961) pointed out that the significant difference between aeolian sand and beach sand is the clay content. The movements of waves maintain the depositional interface perturbation and the clay in a suspended state without leaving deposits on the beach, although wind can transport these fine-grained materials. Therefore, we speculate that this suspended component (grain size < 0.63 μm) was transported from the Asian inland deserts by high-altitude westerly winds, with the MDS as the dust precipitation environment (Sun et al. 2002, 2004). Given that the thin-grain component shear-rate threshold value is less than that of the general atmospheric circulation, the particles can flow into the atmosphere for long periods of time and become dispersed to form atmospheric dust, and they eventually precipitate or get deposited (Ashley 1978). The grain size is consistent with the slow radial variation shown as smaller grain size from the deserts of China and the Loess Plateau in the North Pacific (Rea 1994).

The amount of fine-grain component such as dust, which becomes sedimentary only by wet deposition, and modern meteorological observation at the MDS indicate that 81% of the local rainfall occurs during the summer monsoon (Shandong Changdao County Compilation Committee 1990). Therefore, we assume the < 0.63 μm grain size fraction to represent the monsoon precipitation index. Silt (> 4Φ) is one of the main sources of material in the MDS. Its relatively larger proportion ranges from 22.8 - 42%, including the grain-size sensitive component 2 shown in Fig. 5b.

Table 1. The relevant parameters of AMS-^{14}C and OSL. (a) AMS-^{14}C ages of some horizons in the Miaodao section and their calibrated results. (b) OSL ages of some horizons in the Miaodao section and their analytical data.

(a)

Horizon and lab record number	Depth (m)	Ages of AMS-^{14}C (ka BP)	Calibrated ages (Cal ka BP)
Unit 15-GZ4217	0.25	2.210 ± 0.30	2.237 ± 0.88
Unit 15-GZ4218	0.50	4.305 ± 0.30	4.862 ± 0.30
Unit 14-GZ4220	0.90	8.065 ± 0.50	8.947 ± 0.18

(b)

Horizon and lab record number	Depth (m)	U (10^{-6})	Th (10^{-6})	K (%)	Total dose [E.D (Gy)]	Annual dose (m Gy)	Water content (%)	OSL (ka)
Unit 12-SY01	1.50	1.8	10.4	1.75	71.05 ± 1.26	3.66 ± 0.3	3.46	19.41 ± 0.26
Unit 11-10G520	2.06	1.43	8.67	1.61	81.20 ± 0.94	3.10	3.69	26.2 ± 0.6
Unit 10-SY 02	2.48	1.7	11.1	1.73	139.75 ± 2.61	3.64 ± 0.3	4.31	38.39 ± 0.57
Unit 8-SY 03	3.02	1.4	9.1	1.78	187.69 ± 3.37	3.36 ± 0.3	4.51	55.84 ± 1.02
Unit 6-10G521	3.60	1.20	7.00	1.85	246.86 ± 3.48	3.01	7.58	82.1 ± 3.5
Unit 3-10G522	5.34	1.02	6.86	1.94	337.69 ± 4.89	3.03	6.73	111.4 ± 5.0
Unit 2-SY 04	5.40	1.5	10.6	1.96	404.39 ± 7.13	3.51 ± 0.3	11.20	115.18 ± 2.43
Unit 2-SY 05	6.30	1.3	7.9	1.29	309.52 ± 5.01	2.40 ± 0.2	11.67	129.05 ± 2.61
Unit 1-10G523	6.44	1.96	8.06	1.57	411.08 ± 9.49	3.02	11.37	136.1 ± 6.3

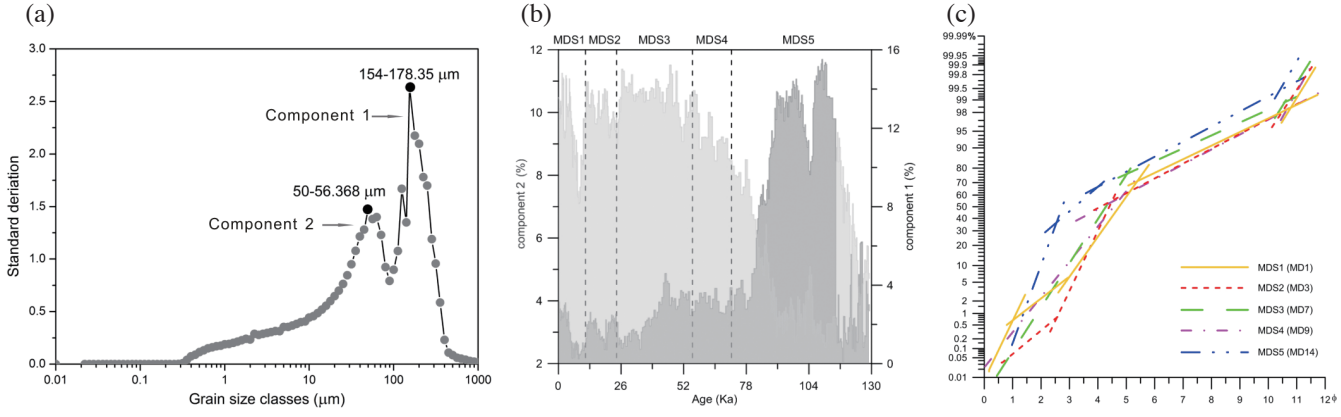

Fig. 5. The grain size characteristics of the MDS. (a) Curve of the size fraction standard deviation. (b) Grain-size sensitive component. (c) The grain-size probability accumulative curves in different subsections. (Color online only)

The grain-size sensitive component 1, also shown in Fig. 5b (1.32Φ to 4Φ), is the other main source for this material. The content changes in the two grain-size sensitive components are complementary to each other. In different depositional phases, these material sources have larger differences that are closely related to sea-level change.

The Bohai Sea has undergone continual sea-level fluctuations since MIS5e (Liu et al. 1987; Fig. 6) leading to differences in the material sources at relatively high and low sea levels. During high sea levels, the main MDS material sources may have been aeolian dune sand that was captured by the Bohai Sea, sand from the North Yellow Sea coast and silt from the Yellow River estuary (Cao et al. 1993). During low sea-level periods, seafloor sediment desertification of the contracted Bohai Sea provided the main source material (Zhao 1991). All of these events occurred during a strong winter monsoon when the suspended silt and sand grains were transported hundreds of meters in the lower troposphere. The sands, with varying levels of coarseness, were transported mainly by saltation and a large amount of accumulated sediment in the downwind area of the source region formed loess. Regardless of whether sea levels were low or high, the MDS sediments were all subject to fluvial transport at first, with subsequent wind transport. Evidence of these transport patterns can be seen in SEM images of the grain surface features (Fig. 7). The quartz in the MDS has significant sphericity and occurs mostly as sub-round to round grains (Powers 1953). Several classical fluviation features can also be observed, such as V-shaped pits and conchoidal fractures. However, the grain edges are frayed

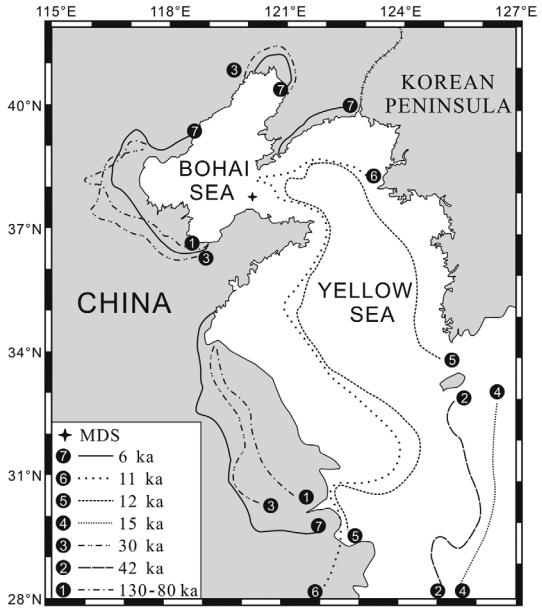

Fig. 6. Sea-level fluctuations in the Bohai Sea since MIS5e.

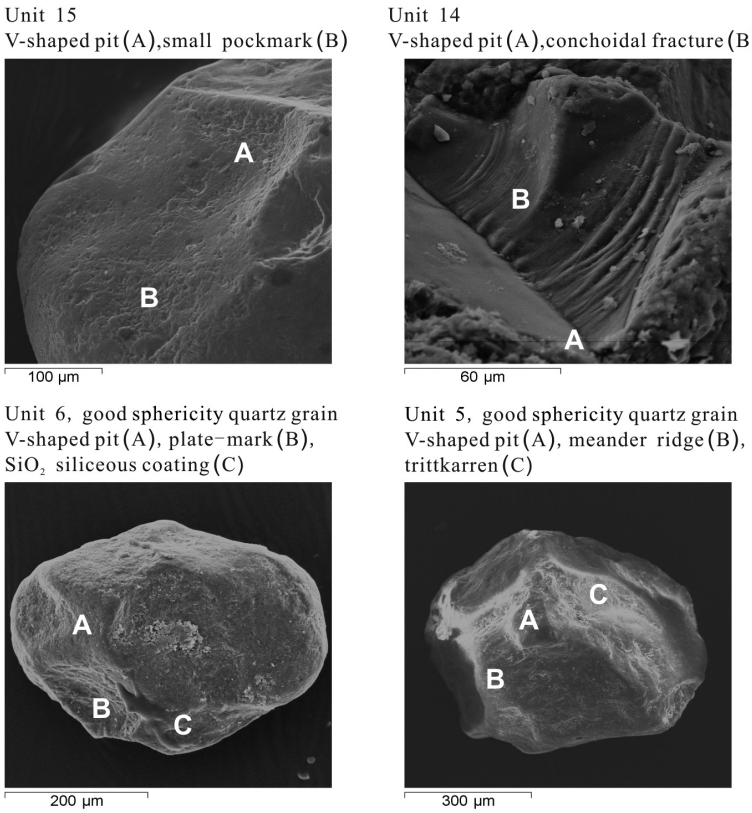

Fig. 7. The scanning electron microscope (SEM) surface textural features of the MDS.

and round, and the fluviation features are overlain with aeolian textural features, including plate marks, meander ridges, trittkarren and SiO_2 siliceous coating. The traction component is mostly under 1%. This part of the sediment source may be local bedrock weathering material.

6.2 East Asian Monsoon Evolution Progress in the Bohai Sea Coastal Zone

6.2.1 Last Interglacial Period

From the bottom to top the five layers in the MDS5 segment (129.1 to 71.2 ka) are Units 2, 3, 4, 5, and 6, which correspond to MDS5e, MDS5d, MDS5c, MDS5b, and MDS5a, respectively. Every paleoclimatic index shows that the climate in the MDS5e segment (113.9 to 129.1 ka) is warm and wet, as shown in Fig. 3. All of the indices appear with their peaks regardless of Mz, SC/D value, < 0.63 μm grain size fraction, CIA value, Rb/Sr ratio, or SiO_2/Al_2O_3 ratio. High Mz and SC/D values indicate that the material in the MDS5e subsection was composed primarily of fine silt, indicating that this layer was deposited during a period of prevailing summer monsoon. High < 0.63 μm grain size fraction, CIA value and Rb/Sr ratio suggest that the climate conditions at that time were very warm and humid. Moreover, an intense level of chemical weathering occurred, resulting in lower SiO_2/Al_2O_3 ratios. A study of this period by Du et al. (2014) found that 5.5 comparable oscillation millennial-scale cold events occurred during the MDS5e deposition. In addition, Fig. 3 shows the monsoon precipitation change curve (< 0.63 μm grain size fraction) indicating possible rainfall fluctuation occurrences, with precipitation peaks in the summer monsoon prevalence period. During these times, the strongest rainfall occurred at approximately 126.21 ka, with a < 0.63 μm grain size fraction peak average of 3.62%. This rate is 2.07% more than the MDS average of 1.55%, of which the approximately 60 a time duration reflects the strongest centennial-scale monsoon precipitation event. This event also recorded the oxygen isotope results from YX21 stalagmites in Shanbao Cave, with an average $\delta^{18}O‰$ of -10.8‰. This value is approximately 1.2‰ lower than the overall $\delta^{18}O‰$ average of -9.6‰ during MIS5e (Jiang et al. 2008). Stalagmite $\delta^{18}O‰$ results in Qixing Cave in Guizhou show the lowest $\delta^{18}O$ value in MIS5e, with an average of -8.67‰. This value is approximately 2.95‰ lower than the $\delta^{18}O$ average of the other stalagmites in this cave. These results show the warmest, most humid and strongest summer monsoon phase in the last glacial-interglacial cycle (Qin et al. 2004). The MDS5d and MDS5b layers, which are composed of aeolian sand accumulation, indicate deposition in a relatively cold and dry climate. The average values for Mz, SC/D, < 0.63 μm grain size fraction, CIA value and Rb/Sr ratio are lower than those for MDS5 and the MDS. The grain size is relatively coarse and the composition is mainly very fine sand. The SiO_2/Al_2O_3 ratio curve shows obvious peaks. The main aeolian sand composition in these layers is quartz. Mineral analysis results indicate a quartz content of more than 40%, which is significantly higher than the 30% found for the MDS5e layer. The climate was warmer and wetter for MDS5a and MDS5c layer development than that for MDS5b and MDS5d layer development in sandy paleosol, although it differed significantly from that for the MDS5e layer. In particular, the sand content was greater and the chemical weathering was less intense, as reflected in the proxy paleoclimatic indices.

6.2.2 Last Glacial Period

The last glacial period in the MDS (71.2 to 11.0 ka) is represented in three segments, MDS4, MDS3, and MDS2, and seven layers. From bottom to top these layers include MDS4 to Unit 7, MDS3c to Unit 8, MDS3b to Units 9 and 10, MDS3a to Unit 11, and MDS2 to Units 12 and 13, which correspond respectively to MIS4, MIS3c, MIS3b, MIS3a, and MIS2 in the time frame. Every MDS climatic index during the last glacial period shows that the sedimentary particles are relatively fine and composed mainly of coarse silt, corresponding to the decline in sea level fluctuation. The exposed bottom sediments are the sources of the MDS. The global climate became cold and dry and the sea level fluctuated many times during the last glacial period. The BQ1 drill core (38°39.883'N, 117°33.808'E), obtained from the Bohai Sea bay on the western shore located in the northwest MDS region, shows that the sea level dropped to -80 m during the MDS4 period (Yan et al. 2006). The monsoon precipitation (< 0.63 μm grain size fraction) was on a declining curve with an average of 1.41%, which is less than the MDS average of 1.55%. The decrease in monsoon precipitation and the cold climate weakened the chemical weathering intensity. The CIA value and Rb/Sr ratio show the lowest peaks, indicating colder conditions than those of the MDS2. These results are similar to the $\delta^{18}O‰$ values of the stalagmites in Qixing Cave (Qin et al. 2004). A sharp decrease in temperature was observed during the last glacial period peak in the late Pleistocene period, resulting in a large volume of accumulated water in glaciers and a sudden decrease in sea level. The global glaciers reached their maximum sizes approximately 18000 years ago, at which time sea level dropped more than -130 m, thereby exposing the Bohai shelves and the Yellow Seas and most of the East Sea shelf. The development of glaciers in the Northern Hemisphere during the pleniglacial period indicates that the winter monsoon strengthened and the air flow was colder and drier. During this time storm, activities were the most important external agent acting upon the continental shelf. Exposure to these storm activities led to continental shelf desertification and accumulation of loess in the desert downwind. The MDS2 layer has higher Mz and CIA values, and the Rb/Sr ratio also peaked in the layer because of the

continental shelf desertification in the Bohai Sea during this period. The sediment from the MDS3a layer was deposited on the MDS2 layer through winter monsoon activity, although the proxy paleoclimatic indices show a considerable influence from the MDS3a layer. Although the strength of the winter monsoon activity was most powerful during this period, a certain amount of summer monsoon activity was still observed. Because the < 0.63 μm grain size fraction indicates a certain degree of monsoon precipitation, Sun et al. (1996) examined the Loess Plateau summer monsoon climate pattern and noted that the summer monsoon reached the Chunhua-Yuexian-Lantian areas in China during the last pleniglacial period, leading to an increase in precipitation, weathering and pedogenesis.

6.2.3 Holocene Epoch

The post-glacial period in the Holocene period (11.0 to 0 ka) deposited two layers of MDS, Units 14 and 15, both of which are silty paleosol. However, these layers differ in paleosol development degree and proxy paleoclimatic indices. Unit 14 was deposited during the Holocene Climatic Optimum. The average Mz, SC/D values, < 0.63 μm grain size fraction, CIA and Rb/Sr ratio in this unit were significantly higher than those for Unit 15, which indicates summer monsoon enhancement. During this period, the argillic soil alteration increased and strong chemical weathering occurred. The < 0.63 μm grain size fraction reflects long-term monsoon precipitation that formed from 11.2 to 7.9 ka and subsequent considerable precipitation intensity with an average of 2.38%, which corresponds to another monsoon period with abundant precipitation after MIS5e. The SB10 $\delta^{18}O‰$ results from the Shanbao Cave stalagmites also indicate that 11.5 to 9.3 ka was a period of heightened monsoon precipitation and that 9.3 to 4.4 ka was a humid period with increased rainfall (Shao et al. 2006). Unit 14 corresponds to an inundation phase in the Holocene with the sea level reaching its maximum 6000 years ago (Zhuang et al. 1991). This maximum sea level was higher than the modern sea level by approximately 3 m. Thereafter, the fluctuations in sea level decreased, although the exposed shelf sediment was continually transported to land by wind erosion to form aeolian dunes or sand layers (Zhang and Yang 1992). When Unit 15 was deposited, the winter monsoon forces were stronger and the summer monsoon forces were weaker, leading to coarse-grained silty paleosol deposition. Thus, the stalagmite $\delta_{18}O‰$ results are obviously biased (Shao et al. 2006).

7. CONCLUSIONS

The results from this study are summarized in the following:

(1) Aeolian sediment deposition since MIS5e on the MDS was driven directly by the East Asian monsoon and source materials caused by sea-level fluctuation. During the high sea-level period (MDS5 and MDS1), paleosols developed as a result of the summer monsoon and indicates a relatively warm and humid climate. The loess and aeolian sand represent the sand production strength during the winter monsoon, indicating a relatively cold and dry climate. During the low sea-level period (MDS4, MDS3, and MDS2), the sediment deposition was influenced mainly by source materials.

(2) The MDS has undergone multiple short-scale, cold-dry and warm-humid climatic fluctuations since MIS5e. During the high sea-level period evidence of abundant rainfall and enhanced chemical weathering were observed in the MDS5e, MDS5c, MDS5a subsections, and MDS1 section, revealing the East Asian summer monsoon strength. During the last glacial period (MDS4 to MDS2), the proxy paleoclimatic indices results indicate influence mainly by source materials, less monsoon precipitation occurred, indicating a weakened summer monsoon.

(3) The < 0.63 μm grain size fraction, used as a monsoon precipitation index, demonstrated the occurrence of multiple rainfall fluctuations in the Bohai Sea coastal zone since MIS5e. Strengthened monsoon precipitation occurred at MDS5e and Unit 14, and the strongest centennial-scale monsoon precipitation event occurred within the MDS5e subsection. Evidence of this latter event can been found in the stalagmite record of the Shanbao Cave. The early Holocene to middle Holocene periods were monsoon periods with persistent precipitation. The rainfall strength was less than that indicated by the MDS5e layer.

Acknowledgements This work was supported by the National Natural Science Foundation of China under Grant (Nos. 41206036, 91228207, 41201006, and 41471159); National Basic Research Program of China (2013CB955903); Guangdong Province Science and Technology Project under Grant (No. 2015A020216015); and by Youth talent forefront project of South China Sea Institute of academy of sciences under Grant (No. SQ201306).

REFERENCES

An, Z., 2000: The history and variability of the East Asian paleomonsoon climate. *Quat. Sci. Rev.*, **19**, 171-187, doi: 10.1016/S0277-3791(99)00060-8. [Link]

An, Z. S., G. Kukla, S. C. Porter, and J. L. Xiao, 1991: Late Quaternary dust flow on the Chinese Loess Plateau. *Catena*, **18**, 125-132, doi: 10.1016/0341-8162(91)90012-M. [Link]

Ashley, G. M., 1978: Interpretation of polymodal sediments. *J. Geol.*, **86**, 411-421, doi: 10.1086/649710. [Link]

Cao, J., G. Liu, N. Shi, Y. Chang, C. Song, H. Yuan, and

X. Guo, 1993: Holocene loess of Miaodao Islands in Shandong. *Quat. Sci.*, **13**, 25-33. (in Chinese)

Chen, J., Z. An, Y. Wang, J. Ji, Y. Chen, and H. Lu, 1999: Distribution of Rb and Sr in the Luochuan loess-paleosol sequence of China during the last 800 ka: Implications for paleomonsoon variations. *Sci. China Ser. D*, **42**, 225-232, doi: 10.1007/BF02878959. [Link]

Dasch, E. J., 1969: Strontium isotopes in weathering profiles, deep-sea sediments, and sedimentary rocks. *Geochim. Cosmochim. Acta*, **33**, 1521-1552, doi: 10.1016/0016-7037(69)90153-7. [Link]

Ding, Z., N. Rutter, J. Han, and T. Liu, 1992: A coupled environmental system formed at about 2.5 Ma in East Asia. *Palaeogeogr. Palaeoclimatol. Palaeoecol.*, **94**, 223-242, doi: 10.1016/0031-0182(92)90120-T. [Link]

Du, S., B. Li, D. Niu, D. D. Zhang, X. Wen, D. Chen, Y. Yang, and F. Wang, 2011: Age of the MGS5 segment of the Milanggouwan stratigraphical section and evolution of the desert environment on a kiloyear scale during the Last Interglacial in China's Salawusu River Valley: Evidence from Rb and Sr contents and ratios. *Chemie Der Erde*, **71**, 87-95, doi: 10.1016/j.chemer.2010.07.002. [Link]

Du, S., B. Li, M. Chen, D. D. Zhang, R. Xiang, D. Niu, X. Wen, and X. Ou, 2012: Kiloyear-scale climate events and evolution during the Last Interglacial, Mu Us Desert, China. *Quat. Int.*, **263**, 63-70, doi: 10.1016/j.quaint.2012.01.004. [Link]

Du, S., B. Li, Z. Li, M. Chen, R. Xiang, D. D. Zhang, D. Niu, and L. Zhang, 2014: Rapid changes in the East Asian monsoon during the Last Interglacial in the Bohai Sea coastal zone, China. *J. Sediment. Res.*, **84**, 88-96, doi: 10.2110/jsr.2014.15. [Link]

Folk, R. L. and W. C. Ward, 1957: Brazos River bar: A study in the significance of grain size parameters. *J. Sediment. Petrol.*, **27**, 3-26.

Jacobs, Z., G. A. T. Duller, and A. G. Wintle, 2006: Interpretation of single grain D_e distributions and calculation of D_e. *Radiat. Meas.*, **41**, 264-277, doi: 10.1016/j.radmeas.2005.07.027. [Link]

Jiang, X., Y. Wang, X. Kong, S. Chen, M. Li, and H. Cheng, 2008: Climate variability in Shennongjia during the Last Interglacial inferred from a high-resolution Stalagmite record. *Acta Sedimentologica Sinica*, **26**, 139-143. (in Chinese)

Konert, M. and J. Vandenberghe, 1997: Comparison of laser grain size analysis with pipette and sieve analysis: A solution for the underestimation of the clay fraction. *Sedimentology*, **44**, 523-535, doi: 10.1046/j.1365-3091.1997.d01-38.x. [Link]

Lai, Z. P., L. Zöller, M. Fuchs, and H. Brückner, 2008: Alpha efficiency determination for OSL of quartz extracted from Chinese loess. *Radiat. Meas.*, **43**, 767-770, doi: 10.1016/j.radmeas.2008.01.022. [Link]

Li, B., D. D. Zhang, H. Jin, Z. Wu, M. Yan, W. Sun, Y. Zhu, and D. Sun, 2000: Paleo-Monsoon activities of Mu Us Desert, China since 150 ka B.P.—A study of the stratigraphic sequences of the Milanggouwan Section, Salawusu River area. *Palaeogeogr. Palaeoclimatol. Palaeoecol.*, **162**, 1-16, doi: 10.1016/S0031-0182(00)00101-2. [Link]

Li, P., X. Xu, and S. Zhao, 2008: The Loess and the Paleo-Glaciation Remains in the Coastal Zone of China, China Ocean Press, Beijing, 337 pp.

Liu, M. H., S. Y. Wu, and Y. J. Wang, 1987: The Late Quaternary Sedimentary in Yellow Sea, China Ocean Press, Beijing, 387 pp.

Liu, T., 1985: Loess and the Environment, Science Press, Beijing, 251 pp.

Pang, J., C. Huang, and Z. Zhang, 2001: Rb, Sr elements and high resolution climatic records in the Loess-Paleosol profile at Qishan, Shannxi. *Acta Sedimentologica Sinica*, **19**, 637-641.

Porter, S. C. and Z. An, 1995: Correlation between climate events in the North Atlantic and China during the last glaciation. *Nature*, **375**, 305-308, doi: 10.1038/375305a0. [Link]

Potter, P. E., 1978: Petrology and chemistry of modern big river sands. *J. Geol.*, **86**, 423-449.

Powers, M. C., 1953: A new roundness scale for sedimentary particles. *J. Sediment. Res.*, **23**, 117-119, doi: 10.1306/D4269567-2B26-11D7-8648000102C1865D. [Link]

Qin, J., D. Yuan, H. Cheng, Y. Lin, M. Zhang, H. Wang, Y. Feng, and L. Tu, 2004: A high resolution late Pleistocene climate-stratigraphy of 4 stalagmites from Qixing cave, Duyun, Guizhou. *Quaternary Sciences*, **24**, 318-324. (in Chinese)

Rea, D. K., 1994: The paleoclimatic record provided by eolian deposition in the deep sea: The geologic history of wind. *Rev. Geophys.*, **32**, 159-195, doi: 10.1029/93RG03257. [Link]

Shandong Changdao County Compilation Committee, 1990: Changdao County Annals, Shandong People Press, Jinan, 22 pp.

Shao, X., Y. Wang, H. Cheng, X. Kong, J. Wu, and E. R. Lawrence, 2006: Long-term trend and abrupt events of the Holocene Asian monsoon inferred from a stalagmite $\delta^{10}O$ record from Shennongjia in Central China. *Chin. Sci. Bull.*, **51**, 221-228, doi: 10.1007/s11434-005-0882-6. [Link]

Shen, J., X. Liu, S. Wang, and R. Matsumoto, 2005: Palaeoclimatic changes in the Qinghai Lake area during the last 18,000 years. *Quat. Int.*, **136**, 131-140, doi: 10.1016/j.quaint.2004.11.014. [Link]

Shepard, F. P., R. Y. Manar, and R. Young, 1961: Distinguishing between beach and dune sands. *J. Sediment. Res.*, **31**, 196-214, doi: 10.1306/74D70B37-2B21-11D7-8648000102C1865D. [Link]

Stuiver, M., P. J. Reimer, E. Bard, J. W. Beck, G. S. Burr, K. A. Hughen, B. Kromer, G. McCormac, J. van der Plicht, and M. Spurk, 1998: Intcal98 Radiocarbon age calibration, 24,000-0 cal BP. *Radiocarbon*, **40**, 1041-1083, doi: 10.2458/azu_js_rc.40.3781. [Link]

Sun, D., X. Wu, and D. Liu, 1996: Evolution of the summer monsoon regime over the Loess Plateau of the last 150 ka. *Sci. China Ser. D*, **39**, 503-511, doi: 10.1360/yd1996-39-5-503. [Link]

Sun, D., J. Bloemendal, D. K. Rea, J. Vandenberghe, F. Jiang, Z. An, and R. Su, 2002: Grain-size distribution function of polymodal sediments in hydraulic and aeolian environments, and numerical partitioning of the sedimentary components. *Sediment. Geol.*, **152**, 263-277, doi: 10.1016/S0037-0738(02)00082-9. [Link]

Sun, D., J. Bloemendal, D. K. Rea, Z. An, J. Vandenberghe, H. Lu, R. Su, and T. Liu, 2004: Bimodal grain-size distribution of Chinese loess, and its palaeoclimatic implications. *Catena*, **55**, 325-340, doi: 10.1016/S0341-8162(03)00109-7. [Link]

Wang, X. F., X. M. Zheng, J. Xu, and F. Liu, 2007: The primary research on magnetic measurements and $CaCO_3$ from Loess sediments of Changdao in Shangdong. *Yunnan Geographic Environment Research*, **19**, 133-138. (in Chinese)

Wang, Y. J., H. Cheng, R. L. Edwards, Z. S. An, J. Y. Wu, C. C. Shen, and J. A. Dorale, 2001: A high-resolution absolute-dated Late Pleistocene monsoon record from Hulu Cave, China. *Science*, **294**, 2345-2348, doi: 10.1126/science.1064618. [Link]

Wen, X., B. Li, S. Li, X. Ou, C. Yao, K. Luo, and L. Zeng, 2005: Grain-size characteristics of Sand Dunes in the Ejin Oasis since 2.5 ka BP and related sedimentary process. *Acta Geol. Sin.-Engl. Ed.*, **79**, 710-718.

Wintle, A. G. and A. S. Murray, 2006: A review of quartz optically stimulated luminescence characteristics and their relevance in single-aliquot regeneration dating protocols. *Radiat. Meas.*, **41**, 369-391, doi: 10.1016/j.radmeas.2005.11.001. [Link]

Xu, S., 2008: Grain size characteristics and its indications of loess in Miaodao Islands, Shandong Province. *Marine Sciences*, **32**, 60-63. (in Chinese)

Xu, S., 2010: Sedimentary characteristics and environmental significance of Loess in Shandong area and comparison with the Loess Plateau during the Last Glaciation. *Ecol. Environ. Sci.*, **19**, 1197-1201. (in Chinese)

Yan, Y. Z., H. Wang, F. L. Li, J. F. Li, C. R. Zhao, and F. Lin, 2006: The sedimentary environment and sea level movements of Borehole BQ1 on the west coast of Bohai Bay. *Geological Bulletin of China*, **25**, 357-382. (in Chinese)

Yuan, D., H. Cheng, R. L. Edwards, C. A. Dykoski, M. J. Kelly, M. Zhang, J. Qing, Y. Lin, Y. Wang, J. Wu, J. A. Dorale, Z. An, and Y. Cai, 2004: Timing, duration, and transitions of the Last Interglacial Asian Monsoon. *Science*, **304**, 575-578, doi: 10.1126/science.1091220. [Link]

Zhang, Z. and Y. Yang, 1992: Features, origins and disaster reduction countermeasures of modern wind-sand hazards in the northern coast area of Jiaodong Peninsula. *J. Desert Res.*, **12**, 34-40. (in Chinese)

Zhao, S., 1991: China shelf sea desertization and its derived deposits during the last stage of late Pleistocene. *Oceanologiaet Et Limnologia Sinica*, **22**, 285-292. (in Chinese)

Zhong, W., J. Xue, Y. Zheng, J. Ouyang, Q. Ma, Y. Cai, and X. Tang, 2010: Climatic changes since the last deglaciation inferred from a lacustrine sedimentary sequence in the eastern Nanling Mountains, south China. *J. Quat. Sci.*, **25**, 975-984, doi: 10.1002/jqs.1384. [Link]

Zhuang, Z., W. Xu, and X. Li, 1991: The coastline evolution on the south coast of the Bohai Sea since 6ka B.P. *Journal of Ocean University of Qingdao*, **21**, 99-110. (in Chinese)